# Unsteady Hypersonic Wake behind Blunt Bodies

J. A. FAY* AND A. GOLDBURG†
*Avco-Everett Research Laboratory, Everett, Mass.*

**Optical observation of wakes behind hypervelocity spheres suggests that large-scale looplike vortex structure is generated in the flow field near the body at characteristic intervals in a phenomenon that bears certain similarities to that which is observed in incompressible flow. Hypersonic wake transition phenomena are examined in the light of this large-scale hypothesis. The quantitative variation of the hypervelocity Strouhal number with Reynolds number shows classical behavior and has an asymptotic limit of about 0.35. In the transition regime, it is suggested that, in schlieren photographs, the distance $x_s$ from the body to the point where some perceptible amount of structure can be seen be interpreted in terms of the distance required for the decay of some amount of fluctuating wake energy from large scale to random small scale. Then, the variation of $x_s$ with $R$ resembles the behavior associated with the development of turbulence in incompressible wakes. A single real gas shoulder Reynolds number of 6000 correlates data for transition to wake unsteadiness in air for $8 < M < 19$. Turbulent core and luminous wake growth for $M > 10$ suggests that for blunt bodies under certain conditions the shock-induced wake independently goes unsteady near to the body rather than being entrained by the turbulent core.**

## A. Introduction: Vortex Loops in Bluff Body Wakes

THE wakes behind hypervelocity bodies during atmospheric re-entry and ballistic range flight can be observed by means of visible radiation. The patterns of observables in the hypersonic turbulent wake may be thought of as being composed in the following schematic way: chemistry determines the observable "tracers," and fluid mechanics determines the mixing patterns. The authors propose to try to advance the understanding of the fluid mechanics of turbulent compressible hypersonic wakes by interpreting the observed patterns of visible radiation in the ballistic range experiments with the aid of what is known about unsteady incompressible wakes.

This paper attempts to show qualitatively and, where possible, quantitatively certain basic fluid mechanical similarities of the incompressible and compressible hypersonic wake. The following points of similarity will be discussed subsequently: 1) characteristic wake disturbance frequency, 2) form of Strouhal number $S$ variation with Reynolds number $R$,‡ 3) coincidence of onset of vortex generation with onset of wake turbulence, 4) correlation of decay of large-scale vortex system into smaller-scale turbulence with Reynolds number, 5) nonaxial symmetry, and 6) wake growth.

These similarities were suggested by comparisons of self-luminous photographs of hypersonic wakes with those of dye-traced incompressible wakes.[1] They are discussed quantitatively in this paper.

The periodic shedding of vortices behind circular cylinders and bluff bodies in subsonic flow at low Reynolds number is a well-known phenomenon. (For a summary, see Goldstein[2] and Torobin and Gauvin.[3]) Roshko[4] with the hot-wire technique examined in detail the shedding and decay of the discrete vortex system behind a cylinder—the von Kármán vortex street—into a fully developed turbulent wake having a continuous energy spectrum. The quantitative evidence developed by Roshko for the vortex shedding and energy decay phenomena consisted of two kinds: 1) the behavior of the nondimensionalized frequency,§ the Strouhal number $S$, with Reynolds number $R$ (Fig. 1); and 2) the develop-

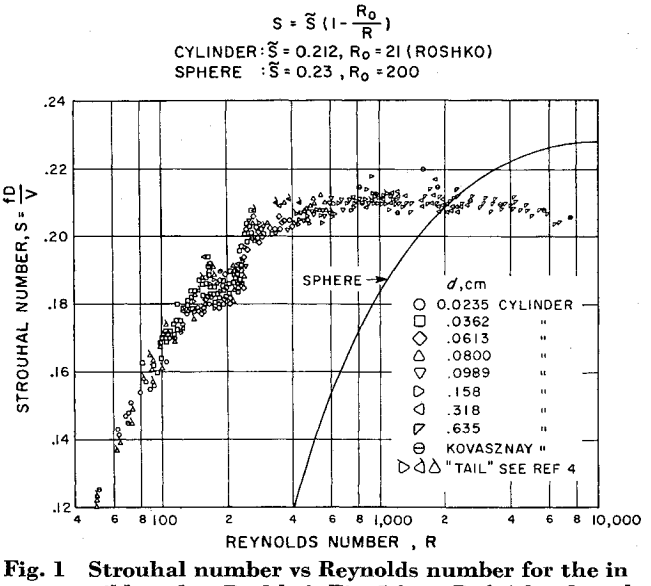


**Fig. 1 Strouhal number vs Reynolds number for the incompressible wake; Roshko's Fig. 5 from Ref. 4 for the cylinder with a curve for the sphere wake calculated from the experiments of Magarvey and Bishop[11] (see Fig. 8).**

Presented at the ARS 17th Annual Meeting and Space Flight Exposition, Los Angeles, Calif., November 13–18, 1962; revision received July 2, 1963. This research was supported jointly by Headquarters, Ballistic Systems Division, Air Force Systems Command, U. S. Air Force, under Contract No. AF 04(694)-33, and by the Advanced Research Projects Agency monitored by the Army Ordnance Missile Command, U. S. Army, under Contract No. DA-19-020-ORD-5476. The authors wish to acknowledge the comprehensive experimental work of their colleagues, R. L. Taylor, J. C. Keck, W. K. Washburn, R. M. Carbone, D. A. Leonard, and B. W. Melcher II, upon which this paper is based. They wish to express their appreciation to the Canadian Armament Research and Development Establishment for providing cooperative use of their ballistic ranges. R. H. Magarvey kindly provided Figs. 7 and 8. V. D. Oppenheimer of the Avco-Everett Research Laboratory Computing Group reduced the wake growth data.

* Consultant; also Professor, Department of Mechanical Engineering, Massachusetts Institute of Technology, Cambridge, Mass. Member AIAA.

† Principal Research Scientist. Member AIAA.

‡ $S$ is defined as the shedding frequency $f$ times the body diameter $D$ divided by the freestream velocity $V$. $R$ is based on diameter unless otherwise stated.

§ One cycle was based on the shedding of every other linear vortex filament.

ment of the ratio of the energy intensity at the shedding frequency and the first harmonic to the total fluctuating wake energy, suitably averaged across the wake, $(E_1 + E_2)/E$, as a function of Reynolds number and distance downstream from the body (Fig. 2). He clearly showed that the generator of and the source of the energy content of the turbulent wake was the vortex system "shed" by the body. Like Roshko, the present authors use the term "shed" throughout the report for convenience; it is not meant to imply anything about the mechanism of the formation of free vortices.

The quantitative evidence in support of the similarities listed previously will be discussed now. Items 1–4 are taken up in Sec. B, and items 5 and 6 are taken up in Sec. D. The evidence leads us to postulate the generation of large-scale vortex structure behind the body as the precursor of turbulence in the hypersonic wake, as is the case for the subsonic wake. The presence of these vortex loop systems in the wake introduces a significant large-scale discrete component to the turbulent wake energy spectrum. Based on knowledge of incompressible cylinder wakes,[4] it is reasonable to expect that as the vortex loops fall further and further behind the body they break down and decay into the smaller-scale random eddies.

## B. Vortex Shedding and Energy Decay in the Hypersonic Sphere Wake

If vortical filaments are formed behind hypervelocity three-dimensional bodies, then it should be possible to find the same sort of quantitative evidence in support of their existence as has been done for the incompressible cylinder case (Figs. 1 and 2).

### 1. Strouhal Number

The Strouhal number depends upon the physical properties of the flow and the geometry of the body surface. Rayleigh[5] first suggested that, for given geometry, an empirical relation existed between the Strouhal and Reynolds numbers of the form

$$S = \tilde{S}[1 - (R_0/R)] \qquad (1)$$

where $\tilde{S}$ is the asymptotic value of the Strouhal number for large $R \gg R_0$, and $R_0$ is the value of the Reynolds number for which $S$ would be zero. Figure 1 shows the experimental points for the incompressible cylinder and the curve for the incompressible sphere wakes. Experimentally, the shedding

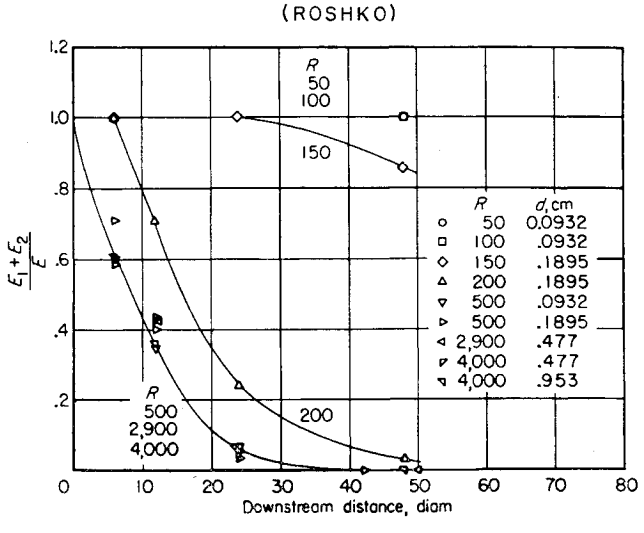


**Fig. 2 Decay of discrete velocity fluctuation wake energy for the incompressible cylinder wake; Roshko's Fig. 13 from Ref. 4.**

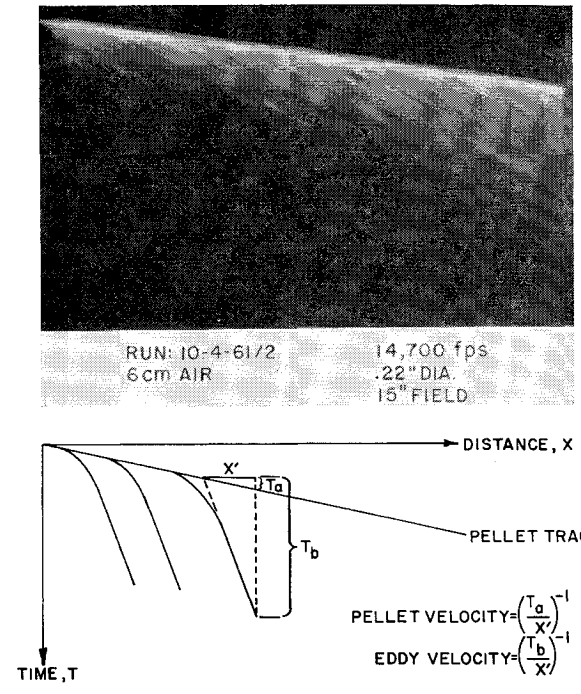


**Fig. 3 Typical drum camera streak photograph with the corresponding space-time plot.**

of vortices is not always apparent for $R \geq R_0$. They usually begin to shed at about $R \geq 2R_0$. For the range $R_0 < R < 2R_0$, the laminar wake may exhibit an undulatory character, unsteadiness, or oscillations of some kind.

The frequency measurements for wakes behind unsaboted hypervelocity spheres ($M_\infty \approx 15$) were made from self-luminous drum camera photographs[6] taken in the Avco-Everett Research Laboratory ballistic range. In the drum camera technique, an open viewing port is used, and the film is moved perpendicular to the direction of flight. Figure 3 is a typical example of a drum camera "streak" photograph. The ablating pellet is moving from left to right and traces the bright, straight line (in the film-pellet geometry, the halo is the less luminous shoulder); the "streaks" are the gross traces of the contaminant-laden vortex filaments, made self-luminous by the highly luminous ablation products, as they fall behind the body and slow down. The resolution of the photographs is to within seven body diameters of the pellet.

The hypersonic Strouhal number is counted by eye in the following manner. A count is made of the number $N$ of prominences along a line of the film parallel to the trace of the pellet. The eye-mind analysis uses two engineering rules. First, it ignores apparent eddy sizes below a certain magnitude. Clearly, luminous fluctuations within a vortex filament are not of interest. Second, obviously, it ignores the length of the data sample as a wavelength of interest.‖ A counting line is chosen as near to the body as the streak structure is resolvable, i.e., immediately downstream of the base resolution limit of the drum camera technique. This choice is made as being the most straightforward one for the eye-mind analysis procedure. If the projectile moves a real distance $x$ in the time during which $N$ events are counted, then the Strouhal number is $ND/x$.

A shoulder Reynolds number is computed (90° from stagnation point) as being representative of the separated flow conditions in the inviscid wake. The best estimates of the flow chemistry indicate an equilibrium flow across the bow

‖ Mechanical procedures for streak counting are being developed. An automatic analysis procedure has the advantage over the eye-mind analysis of incorporating the engineering rules for counting in a known quantitative manner in the filters.

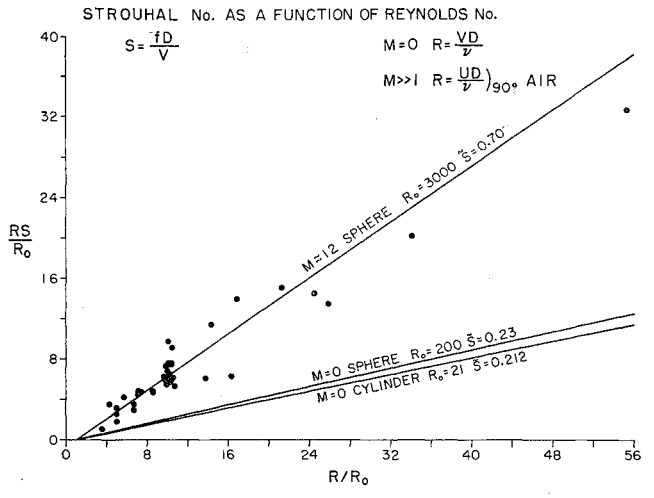


**Fig. 4 $RS$ vs $R$ (shoulder $R = [VD/\nu]_{90°}$) for the hypersonic ($M_\infty \approx 15$) sphere wake in air.**

shock for the ballistic range conditions of these runs. If $p$ is the initial pressure (cm Hg) and $V$ is the flight velocity, these assumptions lead to the following formula for the shoulder Reynolds number in air:

$$R = 1780[V(\text{kft/sec})]^{0.6}[p(\text{cm})][D(\text{cm})] \qquad (2)$$

The Strouhal number plot for hypervelocity pellets ($V$ about 15,000 fps) in air is shown in Fig. 4, where it is compared with the incompressible results.

The constants in the Rayleigh correlation, Eq. (1), for the hypersonic wake data are $R_0 = 3000$ and $\tilde{S} = 0.70$. The value of $R_0 = 3000$ is obtained by taking $\frac{1}{2}$ of the Reynolds number at which vortex structure first appears in the drum camera photographs (see Sec. D on transition). The mechanics of counting were set up such that every luminous prominence was counted and was associated with one cycle of the shedding phenomenon. This is in contradistinction to the practice in the incompressible cases where two vortex filaments were associated with one cycle of the shedding phenomenon. Thus, in making a comparison with the incompressible results, the $\tilde{S}$ should be divided by two. There seems little doubt that in the hypersonic case the magnitude of these dimensionless frequencies in the wake and their dependence upon Reynolds number both follow the pattern observed in incompressible flow. The fact that $\tilde{S}$ and $R_0$ are so little different at Mach 15 from their values at $M \ll 1$ is indeed remarkable. For these reasons alone it seems very likely that large-scale vortices are generated behind bluff bodies in hypersonic flow and, as in the incompressible case, are the major disturbances that initiate a turbulent growth of the wake.

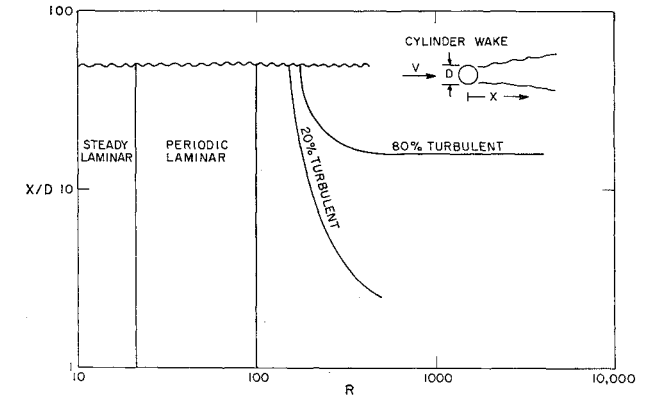


**Fig. 5 Percent of velocity fluctuation wake energy in small-scale random turbulence as a function of $x/D$ and Reynolds number for incompressible cylinder wake (after Roshko[4]).**

In any attempt to proceed further and establish a phenomenology of vortex generation, it is important to note that in the incompressible case the larger part of the drag is in the momentum defect produced by the discrete vortex systems. In the hypersonic case, almost all of the drag is in the momentum defect produced by the shock.

### 2. Energy Decay Lengths for the Discrete Vortex System

Of particular interest is the decay of the fraction: the ratio of the energy spectral intensity at the shedding frequency and the first harmonic to the total fluctuating wake energy intensity, $(E_1 + E_2)/E$, where $E = E_1 + E_2 + E_r$, and $E_r$ is the energy intensity in all other frequencies. In the incompressible case, higher harmonics were found to make negligible contributions to the discrete components.

With hot-wire techniques, Roshko measured the variation of this fraction with Reynolds number and distance downstream for the incompressible cylinder wake (Fig. 2). Figure 5 is a replotting of these data, where "% turbulent" refers to the fraction $E_r/E = 1 - [(E_1 + E_2)/E]$. At fixed $R$ and proceeding downstream to greater and greater values of $x/D$, one transverses a path over which the energy in the periodic velocity fluctuations at the shedding frequency and the first harmonic is continually being transferred down to the energy in the random small-scale eddy velocity fluctuations containing all frequencies. In other words, as one proceeds downstream one will observe that the large-scale discrete linear vortices continually fill up with and are eventually totally consumed by the random small-scale turbulent eddies. The authors believe that there is evidence in schlieren photographs of the hypersonic counterpart of this energy decay process.

A schlieren system has a definite sensitivity limit that is set by the refinement of its optics and the refractivity of the medium. For a given system and a given medium, the contrast in the schlieren image goes as the density gradients along the respective light paths through the medium. Ballistic range experiments in the transition regime for hypersonic wakes in air are performed at densities so low that the finest air schlieren systems are operating close to their sensitivity limit.[7-9] The air schlieren photographs obtained in the transition regime show a more or less smooth texture in the upstream part of the hypersonic wake going over into

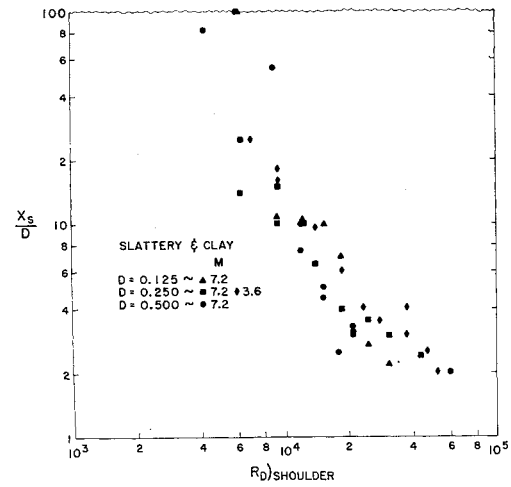


**Fig. 6 Distance $x_s$ from the ball to the point in the wake where some perceptible amount of structure is seen in the schlieren photograph as a function of shoulder Reynolds number, according to the measurements of Slattery and Clay.[8,9] This is interpreted in terms of the distance required for the decay of the large-scale vortex system into some amount of random small-scale turbulence. The wavy line indicates the downstream limit of the experiments.**

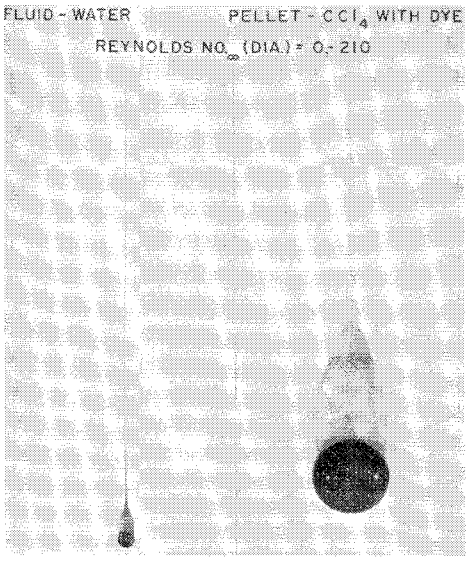


**Fig. 7 Incompressible single thread wake (Magarvey and Bishop[12]).**

a rough eddylike structure towards the downstream part of the wake. This respective absence and presence of contrast is probably not due to a change in fluid mechanical behavior from steady to turbulent flow but due to whether the density gradients in the already unsteady flow starting near to the body are less than or greater than the requisite magnitude for registering the flow pattern on the schlieren photograph.

It is hypothesized that in the transition regime the air schlieren photographs reveal unsteadiness when the large vortex system generated near to the body breaks down and decays into the smaller eddies that produce sufficient sharpness of density gradients for observation with the threshold level of the given schlieren system. Slattery and Clay[8, 9] carefully analyzed their schlieren photographs of hypersonic wakes in the transition regime. For each ballistic range shot (given pressure, velocity, and ball diameter) by eye, they measured the distance $x_s$ from the body to the point where some perceptible amount of structure could be seen in the schlieren photograph.

The data of Slattery and Clay are considered in the sense of locating the position of some given (but unknown) percentage of small-scale turbulence in the hypersonic wake generated by the decay of the large-scale system. Thus, the behavior of $x_s$ as a function of $R$ (Fig. 6) should have the same form as one of the "% turbulent" curves for Roshko's data (Fig. 5). A comparison of the figures indicates that such a similarity exists.

In this section a start has been made at providing quantitative evidence of hypersonic vortex "shedding" of the same type as has been provided for the incompressible wakes. It has been shown in the hypersonic case that the magnitude of the dimensionless "shedding" frequencies and the dependence upon Reynolds number (Fig. 4) both follow the pattern observed in incompressible flow. It has been suggested that the "shed" vortex filaments break down and decay into smaller-scale random eddies as they fall further and further behind the body and that this decay behaves with $x/D$ and $R$ in the same manner as in the incompressible case, Figs. 6 and 5, respectively.

## C. Hypersonic Flow Visualization

Flow visualization is a classical hydrodynamic research tool. It suffers mainly from the necessarily subjective eye-mind analysis interpretative process. Nevertheless, it holds an historically respected position due to its proven usefulness.

Recently, visual flow records of incompressible wakes behind spheres have been obtained. The experiments of

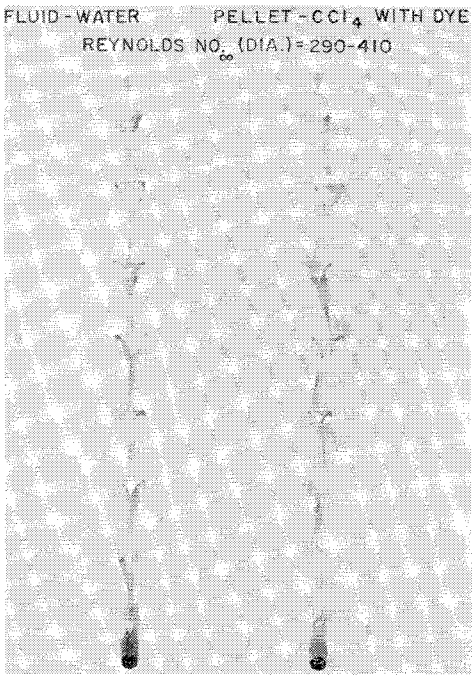


**Fig. 8 Incompressible vortex loop wake (stereo pair); Magarvey and Bishop.[11]**

Magarvey and Bishop[10–12] detail incompressible wakes behind immiscible spherical dye drops falling through water. The dye traces the fluid that streams off the body, allowing examination of the motion set up in the wake. Instantaneous photographs of these incompressible wakes are presented in each reference cited. Six distinct regimes of flow for these incompressible wakes can be delineated[12]: class I, single thread; II, double thread; III, double thread with waves; IV, procession of vortex loops; V, double row of vortex rings; and VI, asymmetrical wake. Figures 7 and 8 are typical of classes I and IV wakes, respectively. The vortex loop sphere wake of Fig. 8 is the three-dimensional counterpart of the von Kármán vortex street behind a cylinder. From a set of such visual observations, a plot of $S$ vs $R$ for the incompressible sphere wake was obtained as shown in Fig. 1.

The vaporized ablation products from an ablating hypervelocity pellet by their self-luminosity trace the fluid that streams off the body. Luminosity is sensitive to temperature. By using xenon as the test gas, very high freestream

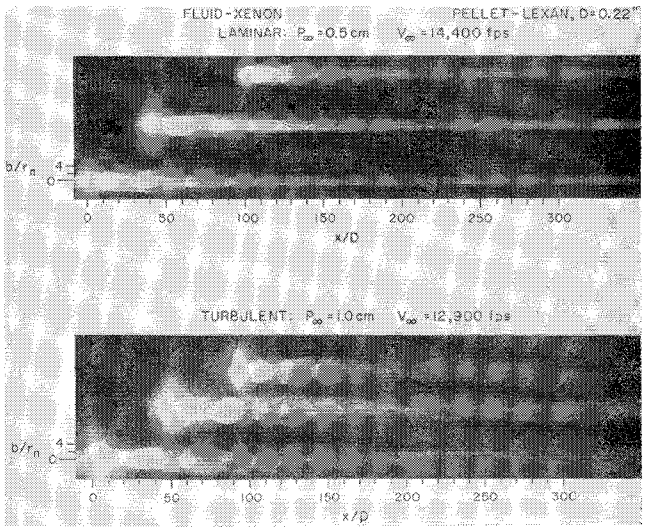


**Fig. 9 Race track photographs of luminous hypersonic ($M_\infty \approx 25$) "single thread" and "vortex loop" wakes; spheres in xenon; 0.22-in. diam; $2r_n = D$; $b$ is half-wake width; multiple images are obtained via a mirror system.[14]**

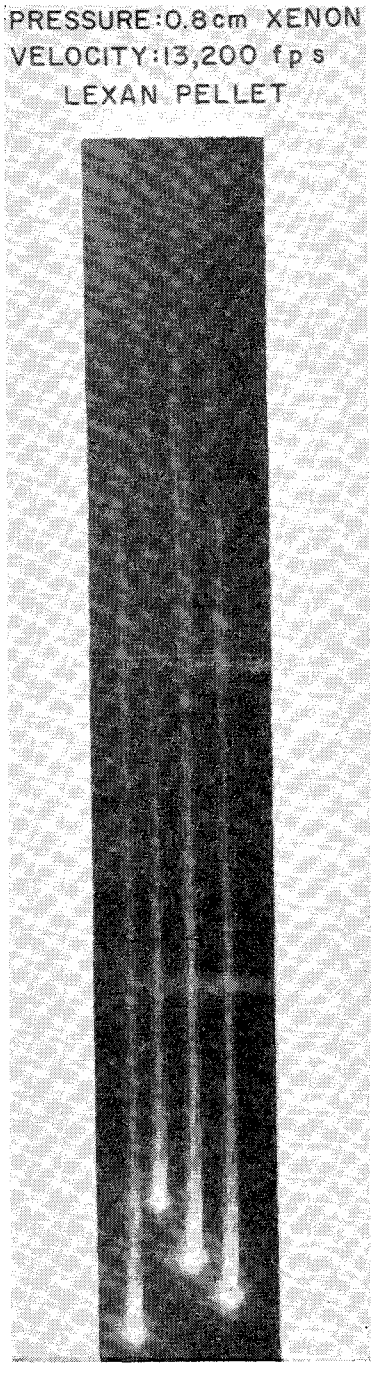


**Fig. 10 Luminous hypersonic undulating wake in the transition regime between the laminar single thread and the fully developed vortex loop wakes; sphere in xenon; 0.22-in. diam.**

Mach numbers are obtained, and hence very high flow-field temperatures are produced behind the bow shock. Figure 9 shows typical "race track" photographs of the self-luminous hypersonic wake behind unsaboted spherical pellets in xenon ($M_\infty \approx 25$). (Additional "race track" photographs of hypersonic wakes may be seen in Ref. 1.) The race track flow visualization technique employed consists of imaging a stationary vertical slit of width of one body diameter on a film in a rotating drum moving with peripheral velocity at approximately the image velocity of the gas particles in the far wake (approximately one-fifth of the pellet velocity).[13, 14] Hence, consecutive parts of the picture are exposed in consecutive instants of time; this is in contradistinction to a spark photograph where all parts of the picture are exposed simultaneously. A major qualitative difference between the race track pictures of the hypersonic wake and the instantaneous pictures of the incompressible wake is the lack of resolution of the body base region in the hypersonic case due to the higher velocities of the body and the near-wake gas particles. Analysis of the race track photographs obtained

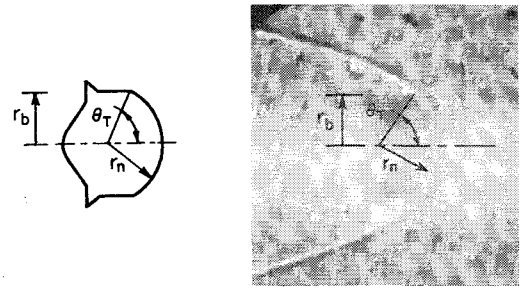


a) b)

**Fig. 11 Sketch and shadowgraph of 0.55-in.-diam quasi-sphere pellet used at CARDE.**

to date appear to show wake flows corresponding to Magarvey and Bishop classes I, II, III, and IV. In each case, the hypervelocity body was an unsaboted spherical pellet. A race track photograph of a hypersonic ($M_\infty \approx 25$) single-thread laminar wake (the halo is interpreted to be hot xenon in the inviscid shock-induced wake) and a hypersonic vortex loop wake, both in xenon, is shown in Fig. 9. The authors suggest that the complexity of the unsteady hypersonic aerodynamic flow field, its representation in a skewed cut across the $x$, $y$-$t$ space,[14] and its visualization only with decaying self-luminous radiation all partially account for the lack of a more direct correspondence to the pattern of the incompressible vortex loop sphere wake as structured in Fig. 8.

## D. Transition and Air Chemistry

The classification of luminous wakes as laminar or turbulent is made on the basis of streak and race track photographs. A laminar wake (e.g., Fig. 9) is one for which there is no modulation of the luminosity in the streak photograph or any asymmetry of the race track pattern. A turbulent wake (e.g., Fig. 9) is one for which either streak or race track photograph shows structure everywhere throughout the whole visible wake. The intermediate case (e.g., Fig. 10) is one for which some structure, usually quite faint, is evident in some part of the wake or some slight asymmetries are noticeable in the race track pictures.

Using this system of classification, the results of firings in air in the Avco-Everett Research Laboratory range (0.22-in.-diam lexan and nylon spheres) and the Canadian Armament Research and Development Establishment (CARDE) range (0.55-in.-diam lexan quasi-spheres, Fig. 11) are summarized in the stability plot of Fig. 12.# For the CARDE experiments, only those runs were accepted for which the monitoring shadowgraphs showed the quasi-sphere to be flying straight and level (Fig. 11). The difference in the quasi-sphere drag coefficient from the sphere value is approximately 25%, which leads to a difference in equivalent diameter based on the square root of $C_DA$ like 10%. The product of ambient pressure (cm Hg) and pellet diameter (cm) for each run is plotted vs flight velocity (kft/sec). At a given flight velocity, for moderate differences in size, the pressure-diameter product is proportional to the Reynolds number and is also the correct scaling parameter for any chemical reaction governed by binary collisions. Since the initial stage of the dissociation behind the bow shock wave is a binary process, this correlation of pressure-diameter product with flight velocity is consistent with both viscous flow effects and dissociation chemistry.

At low velocities and pressures, the dissociation across the bow shock is too slow to be completed before the flow expands around the sphere. At sufficiently high pressure and velocity, however, thermodynamic equilibrium will be achieved within the shock layer at the stagnation point.

# In the preliminary version of this paper, Avco-Everett Research Laboratory Res. Note 295, the CARDE data points are misplotted.

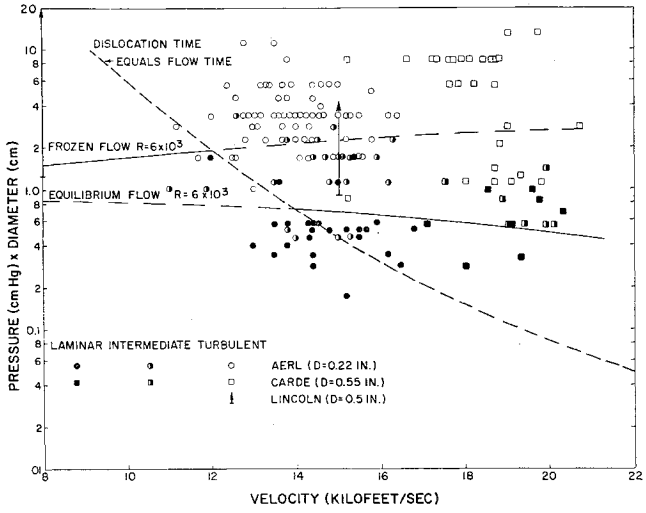


**Fig. 12 Experimental conditions for laminar and turbulent wakes behind spheres and quasi-spheres (CARDE) in air.**

The demarcation between equilibrium and frozen flow across the bow shock occurs for the flight conditions for which the flow time (diameter divided by flight velocity) equals the dissociation time behind a normal shock wave. Making use of the binary scaling of the dissociation process, the test conditions for equal flow and dissociation times were calculated on the basis of Wray's solutions[15] for the time to achieve 70% dissociation behind a plane shock wave. These conditions are shown by the dashed curve in Fig. 12. It can be seen that transition to turbulence and the transition from frozen to equilibrium flow are nearly coincident for flight velocities between 12 and 14 kft/sec.

To correlate transition data, the shoulder flow conditions along the stagnation streamline (90° from the stagnation point) and the sphere diameter have been selected arbitrarily in defining a Reynolds number for the flow typical of the near wake. For a given flight velocity and pressure, the Reynolds number so computed for a completely frozen flow is less than that for a completely equilibrium flow, because, in the former case, the density is lower, whereas the temperature (and hence viscosity) is higher. This effect of chemistry becomes greater at higher velocities but exists even at lower velocities (8 kft/sec) if there is a vibrational heat capacity lag. For the velocity range between 10 and 20 kft/sec in air, the Reynolds number for frozen flow was calculated to be

$$R = 14{,}800[V(\text{kft/sec})]^{-0.6}[p(\text{cmHg})][D(\text{cm})] \qquad (3)$$

For frozen flow, the decrease of Reynolds number with increasing velocity is because the temperature and viscosity increase more rapidly than the velocity. The equilibrium flow Reynolds number is given in Eq. (2).

Lines of constant Reynolds number of 6000 are plotted in Fig. 12. It is seen that this value gives perhaps the best average demarcation between laminar and turbulent wakes. At velocities less than 12 kft/sec, transition occurs at a frozen Reynolds number of about 6000. At velocities about 14 kft/sec, transition occurs at an equilibrium Reynolds number of about 6000. At intermediate velocities, transition occurs under conditions for which the bow shock chemistry changes from frozen to equilibrium, raising the Reynolds number as equilibrium is achieved. The minimum pressure at which some turbulence was noted in sphere wake schlieren photographs by Slattery and Clay[8,9] is also plotted in Fig. 12 and agrees with the transition Reynolds number of about 6000. Data similar to those shown in Fig. 12 have been obtained for hypervelocity spheres in argon and xenon.[16] A Reynolds number of 2000 is found to demarcate transition for these gases. Thus, reasonably good correlation exists to a factor of three among all three gases on the basis of Reynolds number alone.

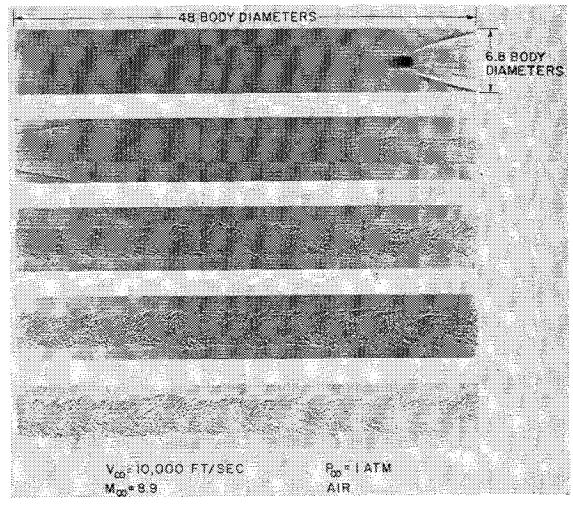


**Fig. 13 Representative shadowgraph of hypervelocity projectile and wake. Exposure time, 1 to 2 μsec; total length of shadowgraph is 480 projectile radii; 0.22-in. diam.**

## E. Growth of Unsteady Luminous Wakes at $M \approx 25$

For a space average of wake growth, one takes a snapshot picture of the wake; Fig. 13 is a spark shadowgraph. Then, one takes local exact data readings of half-wake width $b$ as a function of distance downstream from the pellet $x$. ($r_n$ is nose radius, and $D$ is diameter.) A quartic fit to such data is a space average and is shown in Fig. 14. For a time average, many such "snapshots" are taken and the results of the data reduction placed on one grid. In Fig. 15, wake growth data from eight shots are plotted for $M \approx 10$ and from five shots for $M \approx 6$. (These data indicate that wake growth is insensitive to Mach number, as is to be expected since turbulent diffusion is a geometric phenomenon, in contradistinction to molecular diffusion, which is controlling in the laminar wake.) A quartic fit to these data is a time average and is also shown in Fig. 15. The root mean square deviation for the time average is about 20%.

In nonhomogeneous turbulence, such as the wake problem, the space average of a property at an instant of time has a different form and a smaller root mean square deviation from the instantaneous values than does the uncorrelated time average. It is important to note that, even for the smaller-scale turbulence to which the shadowgraph system is sensitive, the spatial wake growth is a broad band of points which shows a significant root mean square deviation

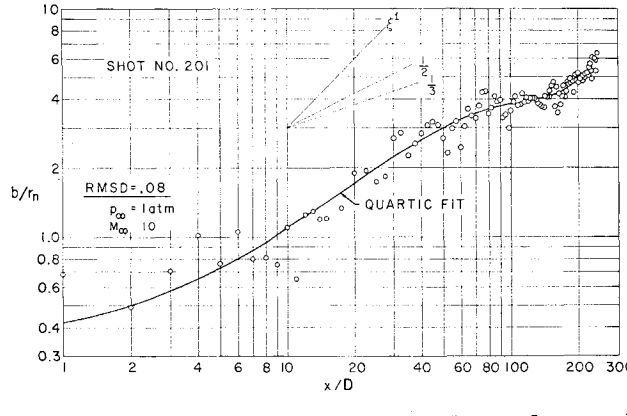


**Fig. 14 Instantaneous hypersonic turbulent wake growth data from a shadowgraph with the space average quartic fit; sphere in air; 0.22-in. diam.**

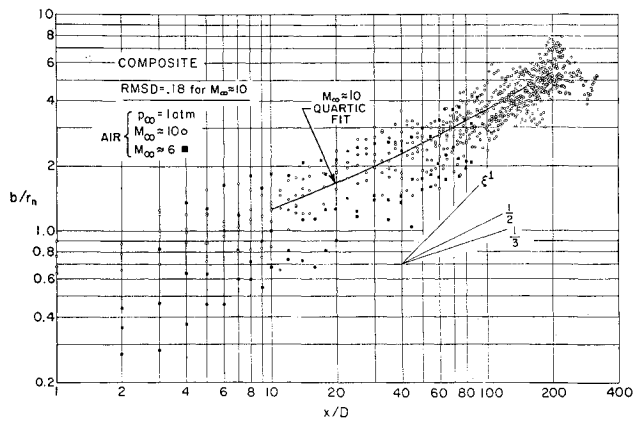


**Fig. 15 Composite of instantaneous hypersonic turbulent wake growth data from eight shadowgraphs at Mach ≈ 10 with a time-averaged quartic fit. Data from five shadowgraphs at Mach ≈ 6 added; spheres in air; 0.22-in. diam.**

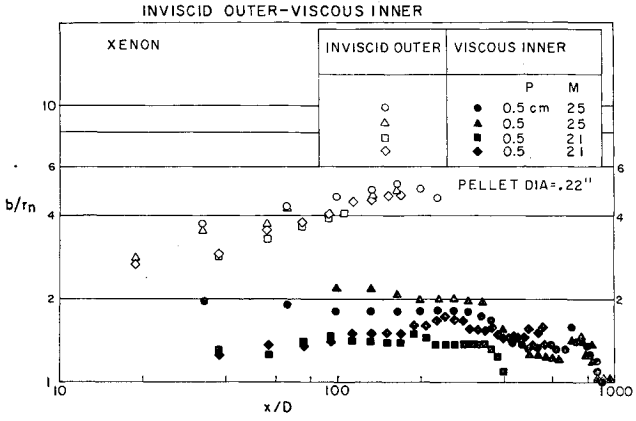


**Fig. 16 Hypersonic luminous laminar wake growth data at Mach ≈ 25 from race track photographs; spheres in xenon; 0.22-in. diam.**

from the time-averaged value represented by the quartic fit. Thus, with respect to any time-averaged representation of wake growth, the actual local instantaneous values of wake width will most likely be different by as much as 25%, a fortiori with respect to local instantaneous values of temperature, density, velocity, pressure, and species and electron concentration.

Next a large number of race track photographs of hypersonic self-luminous turbulent wakes at Mach 25 are considered (see, for example, Fig. 9). The data are obtained by mechanically marching downstream and measuring local "exact" wake widths. Measurement begins where the race track photograph is resolvable (see Sec. C and Ref. 14). Figure 9 indicates that there is subjectivity in the determination of the local extent of the luminous wake. Nevertheless, there was a remarkably close agreement (within 10%) of the same readings made by different observers. To minimize observer bias in the extraction of these data, several different observers were used for different runs.

At the very high Mach ≈ 25 which is obtained with the use of xenon gas, both the boundary-layer-induced inner core and the hot-gas shock-induced inviscid outer (sometimes called "entropy") wake are self-luminous; Fig. 9 shows a race track photograph for the laminar case in which both wakes are visible. Figure 16 is a plotting of the two laminar wake growths for xenon. The falling off of $b/r_n$ at large $x/D$ is due to the fading of the self-luminosity as the temperature drops. Also shown in Fig. 9 is a race track photograph for the turbulent wake with apparent width as large as that of the luminous outer wake of the laminar case. Figure 17 is the composite plot of the data of wake growth for both the luminous laminar outer wake and luminous turbulent wake. It is seen that the extent of the luminous turbulent wake is very nearly that of the luminous outer wake, thus giving initial turbulent wake sizes of the order of the size of the hot-gas shock-induced outer wake, which is about a factor of 2 or more larger than the boundary-layer-induced inner core in the near-wake region. This fact seems to indicate in the regime of the very high Mach numbers near to 20 and 25 and very low transition pressures (Reynolds numbers) that both the boundary-layer-induced inner wake and the hot-gas shock-induced outer wake go into unsteady motion together, starting very near the body. Indeed, one race track photograph in the transition regime between the laminar wake and the fully developed vortex loop wake, shown in Fig. 9, shows both wakes shaking or undulating independently of each other (see Fig. 10).

Measurement of schlieren photographs for wakes in the transition regime (Fig. 10 of Ref. 8) indicates an explosive growth of the wake immediately downstream of the expansion region ($p = p_\infty$ point). The explanation suggested here is that the shock-induced wake is already in small amplitude unsteady motion with density gradients too small to be observed by the schlieren system. The apparent explosive growth occurs where the density gradients in the outer wake become sufficiently large to register on the schlieren photograph. This fluid mechanical behavior is in contradistinction to the Lees and Hromas[17] conceptualization of turbulent hypersonic wake growth which looks upon wake growth as a steady entraining of the outer laminar wake by the inner

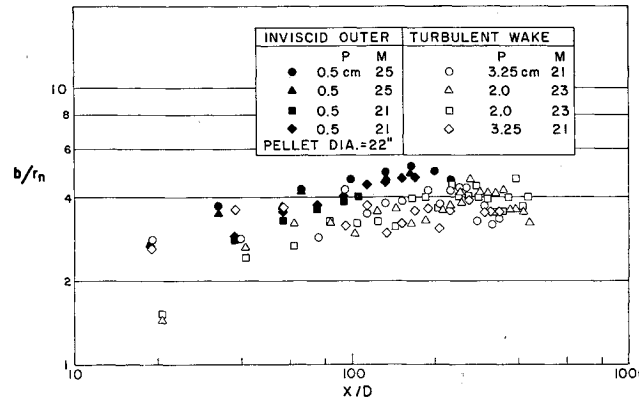


**Fig. 17 Comparison of luminous shock-induced inviscid outer wake growth data and luminous turbulent wake growth data at Mach 25; spheres in xenon; 0.22-in. diam.**

turbulent core based upon a similarity assumption for the turbulent diffusion process; and, in fact, their growth theory does not agree in the near wake where the explosive growth occurs with the experimental results (Fig. 9 of Ref. 17). It is possible that, in the regime of the higher Mach numbers and transition Reynolds numbers, the wake flow can be more appropriately considered to be similar to that of the flow of hot gas in a pipe, the cooler dense surrounding gas acting as the walls of the pipe.

Race track photographs have been taken simultaneously in two different planes providing a top and side view of the turbulent wake. Figure 18 shows such a set of race track pictures for an air turbulent wake. Figure 19 presents the turbulent wake growth measurements for the race track photographs of Fig. 18. The results confirm the asymmetry evident to the eye. Data have been taken from many sets of orthogonal pictures, and an asymmetry in the wake growth is usually evident. This suggests that turbulent wakes behind axially symmetric bodies are not usually axially symmetric. If the luminous turbulent wake contains large-scale horseshoe-like vortex loops (see Secs. A, B, and C), then it is expected that the extent of the luminous turbulent wake will appear to have different magnitudes, depending on the

viewer's position with respect to the spatial orientation of the loops. Also, as the energy in the fluctuating velocity is passed down from the large-scale into the better-mixed smaller-scale random eddies, then the better mixing accomplished by the smaller-scale eddies should reduce the asymmetries in the wake flow field and effect a trend toward axial symmetry with distance downstream. Such a trend is evidenced by a merging together of the orthogonal growth curves that can be seen in Fig. 19. These remarks about the nonaxial symmetry of the hypersonic wakes are equally applicable to the incompressible wakes of Refs. 10–12.

Finally, reference is made to the incompressible vortex loop wake. Figure 20 is a plotting of wake growth data from Refs. 10 and 11 taking the local extreme extent of the particular vortex loop as the size of the wake. It is interesting to note that shedding of the vortex loops induces velocity fluctuations in the incompressible wake flow field which give rise to a growth behavior for the vortex loop wake which is like that predicted and observed for turbulent wakes in general,[18] that is, $b \propto x^{1/3}$. The dotted line is a fit to the hypersonic data of Fig. 15.

## F. Use of an Ablating Body

All of the self-luminous hypersonic wake data used in this study of the unsteady wake were obtained with ablating

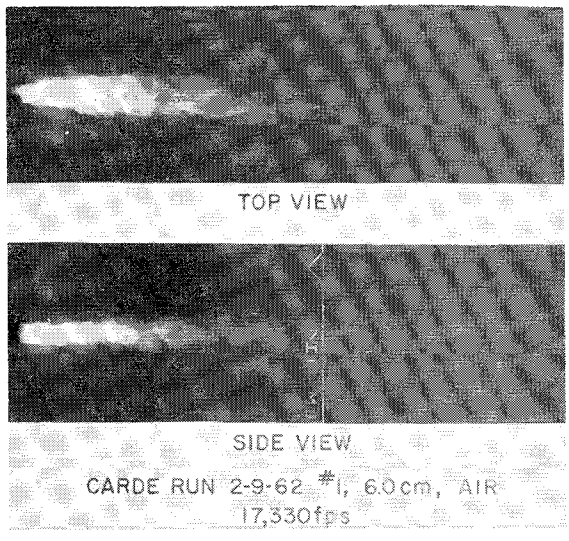


**Fig. 18 Orthogonal race track photographs of a hypersonic wake; quasi-sphere in air; 0.55-in. diam.**

bodies. The vaporized ablation products provide luminous signals well above the threshold values of the diagnostic instruments. Since it is the characteristics of the unsteadinesses which are being detailed, the question naturally arises as to whether the ablation process itself is unsteady, thereby contributing spurious signals to the observed phenomenon under experiment.

Calculations showed that the time to reach steady-state ablation[19] for a rotating pellet was less than the time of flight to the first observation station. Calculations also showed that the pellet could not rotate and maintain its structural integrity at the frequencies associated with the large-scale vortex formation: $f \approx 0.5 \times 10^6$ cps. Furthermore, monitoring shadowgraphs showed that the pellets maintained their spherical shape. Thus, it is felt that the ablation process did not affect the experimental techniques used to observe the unsteady fluid mechanical flow fields.

## G. Conclusions

1) Transition for hypersonic wakes behind spheres is associated with a vortex formation with characteristic frequencies which accompanies the development of a turbulent wake.

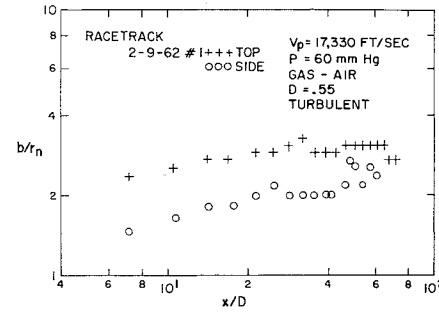


**Fig. 19. Hypersonic luminous turbulent wake growth data from the orthogonal race track photographs of Fig. 18.**

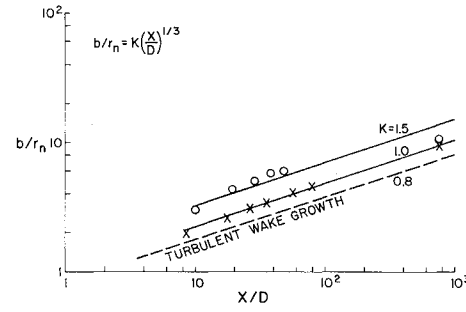


**Fig. 20 Incompressible vortex loop wake growth data based on Refs. 10 and 11. "Turbulent wake growth" is the time-averaged quartic fit to the hypersonic data of Fig. 15.**

2) For spheres, the transition from a laminar wake to an unsteady wake with vortex "shedding" depends almost entirely upon the Reynolds number (suitably evaluated in the flow downstream of the bow shock wave, including the effects of gas chemistry) and very little upon the Mach number in the range $10 < M < 20$.

3) For Mach number about 20 and for Reynolds number (freestream pressure) near to the transition value, the lateral extent of the turbulent luminous wake about 20 diam behind the sphere is close to that of the hot-gas shock-induced entropy wake, indicating the unsteadiness of the whole hot-gas shock-induced wake close behind the body.

4) The many points of similarity, listed in the Introduction, between incompressible and hypersonic wakes suggest the need to incorporate the unsteady, nonaxisymmetric vortex generation phenomena into near-wake flow and wake development theories.

## References

[1] Goldburg, A. and Fay, J. A., "Vortex loops in the trails behind hypervelocity pellets," ARS J. **32**, 1282–1283 (1962).

[2] Goldstein, S., *Modern Developments in Fluid Dynamics* (Oxford University Press, Oxford, 1938), Chap. XIII.

[3] Torobin, L. R. and Gauvin, W. H., "The sphere wake in steady laminar fluids," Can. J. Chem. Eng. **37**, 167–176 (1959).

[4] Roshko, A., "On the development of turbulent wakes from vortex streets," NACA Rept. 1191 (1954).

[5] Rayleigh, L., "Aeolian tones," Phil. Mag. **29**, 433–453 (1915).

[6] Hidalgo, E., Taylor, R. L., and Keck, J. C., "Transition in the viscous wake of blunt bodies flying at hypersonic speeds," J. Aerospace Sci. **29**, 1306–1315 (1962).

[7] Leonard, D. A. and Keck, J. C., "Schlieren photography of projectile wakes using resonance radiation," ARS J. **32**, 1112–1114 (1962).

[8] Slattery, R. E. and Clay, W. G., "Measurement of turbulent transition, motion, statistics and gross radial growth behind hypervelocity objects," Phys. Fluids **5**, 849–856 (1962).

[9] Slattery, R. E. and Clay, W. G., "Laminar-turbulent transition and subsequent motion behind hypervelocity spheres,"

ARS J. 32, 1427–1429 (1962).
[10] Magarvey, R. H. and Bishop, R. L., "The wake of a moving drop," Nature 188, 735–736 (1960).
[11] Magarvey, R. H. and Bishop, R. L., "Wakes in liquid-liquid systems," Phys. Fluids 4, 800–805 (1961).
[12] Magarvey, R. H. and Bishop, R. L., "Transition ranges for three-dimensional wakes," Can. J. Phys. 39, 1418–1422 (1961).
[13] Allen, W. A., Rinehart, J. S., and White, W. C., "Phenomena associated with the flight of high speed pellets," J. Appl. Phys. 23, 132–137 (1952).
[14] Washburn, W. K. and Keck, J. C., "The race track flow visualization of hypersonic wakes," ARS J. 32, 1280–1282 (1962).
[15] Wray, K. L., "Chemical kinetics of high temperature air," Avco-Everett Res. Lab. Res. Rept. 104 (June 1961); also *ARS Progress in Astronautics and Rocketry: Hypersonic Flow Research*, edited by F. R. Riddell (Academic Press, New York, 1962), Vol. 7, pp. 181–205.
[16] Fay, J. A. and Goldburg, A., "The unsteady hypersonic wake behind spheres," Avco-Everett Res. Lab. Res. Rept. 139 (November 1962).
[17] Lees, L. and Hromas, L., "Turbulent diffusion in the wake of a blunt-nosed body at hypersonic speeds," J. Aerospace Sci. 29, 976–993 (1962).
[18] Schlichting, H., *Boundary Layer Theory* (McGraw Hill Book Co. Inc., New York, 1955), Chap. XXIII.
[19] Brogan, T. R., "Electric arc gas heaters for re-entry simulation and space propulsion," Avco-Everett Res. Lab. Res. Rept. 35 (September 1958).

OCTOBER 1963 AIAA JOURNAL VOL. 1, NO. 10

# Magnetohydrodynamic Flow Past a Wedge with a Perpendicular Magnetic Field

YOICHI MIMURA*
*Cornell University, Ithaca, N. Y.*

**The magnetohydrodynamic two-dimensional steady supersonic flow past a wedge with attached straight shock waves is investigated. The fluid is assumed to be nonviscous and perfectly conducting. The wedge is nonconducting, nonmagnetic, and symmetric with respect to the flow. The magnetic field is applied perpendicular to the uniform flow. The general procedure to obtain the solution with two kinds of attached straight shock waves is studied for an arbitrary Mach number (>1) and an arbitrary strength of the magnetic field. The approximate solutions for the case of weak magnetic field and for the case of the small-angle shock waves are treated. The analysis shows that the hydrodynamic shock wave does not change its position and strength in the first order of the foregoing approximation. However, when the weak magnetic field is applied, the new magnetohydrodynamic shock wave appears near the surface of the wedge, and it leaves the surface as the magnetic field increases; for a further increase of the magnetic field, it meets the hydrodynamic shock wave, and then the solution with attached shock wave disappears. For a still stronger magnetic field, the magnetohydrodynamic shock wave appears in front of the hydrodynamic shock wave.**

## 1. Introduction

THE magnetohydrodynamic two-dimensional steady supersonic flow past a wedge with attached straight shock waves is investigated. The fluid is nonviscous and perfectly conducting. The wedge is insulated and nonmagnetic; it is placed symmetric to the flow. The magnetic field is applied perpendicular to the uniform flow. Kogan[1] and Chu[2] treated this problem including unsymmetric flows with the linearized theory. They obtained solutions with two kinds of attached waves. The nonlinear problem is treated here for an arbitrary Mach number (>1) and for arbitrary magnetic field strength.

## 2. Helfer's Treatment of a Shock Wave

The relations between the physical quantities across the shock waves in a perfectly conducting, compressive, nonviscous fluid are determined. Following de Hoffman and Teller,[3] the flow velocity is made parallel to the magnetic field by using a coordinate system moving parallel to the shock front.

The $y$ axis is chosen parallel to the shock front and is pointed toward the apex of the wedge, and the $x$ axis is perpendicular to the $y$ axis and pointed toward the wedge. Then the coordinate system on the lower side of the wedge is a right-hand one (Fig. 1). Physical quantities in front of and behind the shock wave are discriminated by the suffixes 1 and 2. The magnetic field is denoted by $\mathbf{B}_i$ ($i = 1, 2$), the angle made by the magnetic field to the normal of the shock front by $\theta_i$, the fluid velocity by $\mathbf{v}_i$, the density by $\rho_i$, the pressure by $p_i$, and the permeability by $\mu$, and it is assumed that $\mu$ is constant (Fig. 2) (mks units are used).

Choosing the coordinate system in which $\mathbf{B}_i$ and $\mathbf{v}_i$ are parallel,

$$B_{iy}/B_{ix} = v_{iy}/v_{ix} \qquad i = 1,2 \quad (2.1)$$

The continuity equations, momentum equations, and energy equation are given by

$$\rho_1 v_{1x} = \rho_2 v_{2x} = k \quad (2.2)$$

$$B_{1x} = B_{2x} \quad (2.3)$$

$$k(v_{2x} - v_{1x}) = (p_1 + B_{1y}^2/2\mu) - (p_2 + B_{2y}^2/2\mu) \quad (2.4)$$

Received June 18, 1963. This study was carried out partly under Contract AF 49(638)-674 monitored by the Mechanics Division of the Air Force Office of Scientific Research. The author would like to acknowledge valuable discussions with W. R. Sears and A. R. Seebass of the Graduate School of Aerospace Engineering, Cornell University, and with Fujihiko Sakao, Aeronautical Research Institute, University of Tokyo, Japan.

* Graduate School of Aerospace Engineering. On leave from Hiroshima University, Hiroshima, Japan; now Professor, Defence Academy, City of Yokosuka, Japan.